Polaron relaxation and variable-range-hopping conductivity in the giant-dielectric-constant material $CaCu_3Ti_4O_{12}$

Lei Zhang[1,2] and Zhong-Jia Tang[1]
[1]*The Center for Materials Chemistry and Department of Chemistry, 136 Fleming Building, University of Houston, Houston, Texas 77204, USA*
[2]*Department of Physics, Shandong University, Jinan, People's Republic of China*
(Received 2 October 2003; revised manuscript received 29 March 2004; published 22 November 2004)

Transport and dielectric measurements have been performed in $CaCu_3Ti_4O_{12}$ ceramics. The bulk ac conductivity shows a power-law behavior at different temperatures, which is related to polaron relaxation. The temperature dependence of the bulk dc conductivity indicates a variable-range-hopping mechanism. The dielectric relaxation frequency deviates from the Arrhenius behavior. An equivalent circuit is used to explain qualitatively the experimental data of $CaCu_3Ti_4O_{12}$.

DOI: 10.1103/PhysRevB.70.174306 PACS number(s): 71.38.Ht, 77.22.Ch, 72.80.Ng

I. INTRODUCTION

High dielectric constant materials have numerous technological applications.[1,2] The perovskite-related bcc material $CaCu_3Ti_4O_{12}$ (CCTO) has generated much interest attributable to its high dielectric constant ε' ($>10\,000$) at room temperature and very small temperature dependence near room temperature.[3–7] Both properties are important for device implementation.[2]

Below 100 K, the dielectric constant of CCTO drops rapidly to a value of $\sim$100. The low-temperature crossover is characteristic of an activated relaxation process.[4,5] Optical conductivity measurements on CCTO single crystals revealed that anomalous behavior is observed in a low-frequency vibration at low temperature, indicating that a redistribution of charge might occur in the structure.[5,8] From density-functional theory, within the local spin-density approximation, the static dielectric constant was calculated to be $\sim$40.[9,10] Thus it has been speculated[9] that the giant dielectric phenomenon in CCTO could originate from an extrinsic effect.

The large ε' for CCTO has been attributed to Maxwell-Wagner-type contributions of depletion layers at grain boundaries, or at the interface between sample and contacts.[11] Recently, a thin insulating aluminum oxide layer has been used to separate the CCTO sample and electrode, and a giant dielectric constant ($\sim 10^4$) was obtained indicating that contact contributions[12] as the source of the giant dielectric constant can be ruled out.[5,13] It has been accepted widely that an internal barrier layer capacitance (IBLC) model is suitable to explain the dielectric behaviors at low temperatures.[3,8,14,15] The basic idea is that the bulk of the material is either conducting or nearly so, and the insulating layers are responsible for the high capacitance. Impedance measurements have shown the existence of the high conduction in the bulk of CCTO ceramics.[16] However, the conducting mechanism is still unclear. In this paper, we will discuss this problem.

An ideal CCTO crystal should be a band insulator. The existence of the actual high bulk conduction means that an obvious defect structure exists in the real system. There are three possible sources contributing to the conduction: ions, electrons, and polarons.[17]

Oxygen vacancies exist generally in pervoskite materials,[18–20] and the motion of oxygen vacancies can induce a high conduction. However, the measurement of the low-temperature dielectric relaxation shows that the activation energy is approximately 54 meV for CCTO,[5] which is much lower than the activation energy for ion jumping (0.2–1 eV).[21] Thus the possibility that the conduction is from ion jumping can be ruled out. For CCTO, the low-temperature relaxation, which is observed to be activated with a frequency of 1 MHz,[4,5] appears to be too slow to attribute directly to an electronic tunneling mechanism.

For perovskite materials, the polaron relaxation exists generally at low temperatures in crystals with defects. Biadault *et al.*[21] have shown that the activation energy of the polaron relaxation is nearly the same ($\approx$75 meV) for all the investigated perovskites regardless of their composition, texture, or dielectric properties. In Fe-doped $SrTiO_3$, polaron relaxation was found to be intimately related to Mott's variable-range-hopping (VRH) conduction.[22] In this paper, our work shows that the Mott's VRH conduction[23] exists in CCTO ceramics at low temperatures. Consequently, the IBLC effects lead to "giant dielectric phenomena" in CCTO. The x-ray photoelectron (XPS) analysis revealed the coexistence of Ti^{3+} and Ti^{4+} ions. The state of mixed valences of Ti ions in CCTO induces the high bulk polaron conduction of grains.

II. EXPERIMENTAL

Single-phase CCTO ceramics were prepared by standard ceramic processing techniques. $CaCO_3$ (Aldrich, 99%), TiO_2 (Aldrich, 99.9%), and CuO (Fisher, 99.7%) were mixed in the appropriate molar ratios, pressed into 0.5-in diameter pellets, and fired for 8 h in dense Al_2O_3 crucibles in air at 1000 °C. The pellets were then reground and repressed into 0.5-in diameter pellets, and heated to 1100 °C for an additional 29 h. The x-ray powder diffraction pattern on the calcined powder could be fully indexed on the reported unit cell.[3] For electrodes, the pellet surfaces were coated with

 ©2004 The American Physical Society

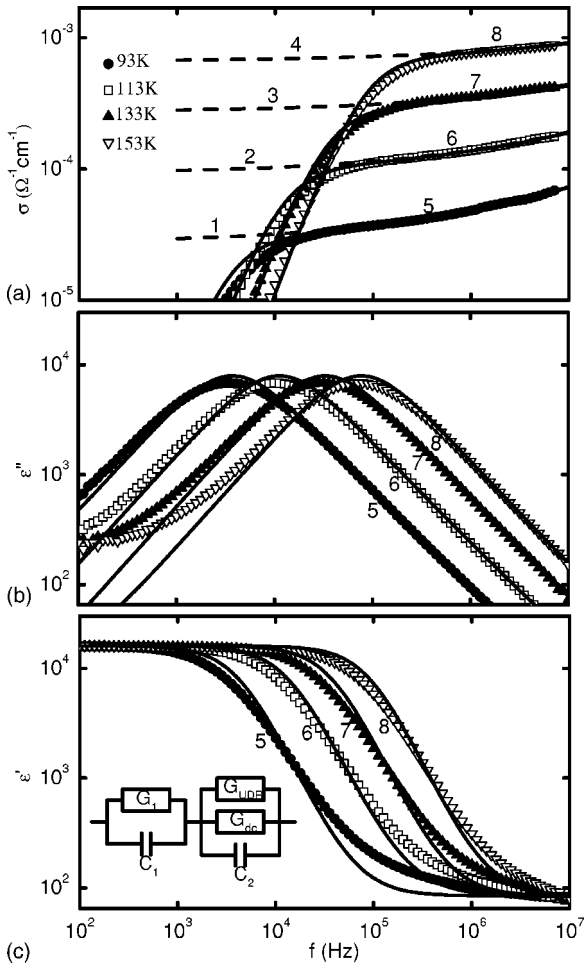

FIG. 1. Frequency dependence of conductivity σ (a), imaginary dielectric permittivity ε'' (b), and real dielectric permittivity ε' (c) of CCTO ceramics at different temperatures. The dashed lines 1–4 are the fit according to Eq. (1). The equivalent circuit in (c) is suggested by Lunkenheimer *et al.* (Ref. 11). The solid lines 5–8 are the calculated results with the equivalent circuit.

air-drying conducting silver paste and cured at 350 °C. The measurements of conductance and capacitance were made on a HP4192a impedance analyzer over the frequency 10^2–10^7 Hz.

III. EXPERIMENTAL RESULTS

Figure 1 shows the frequency dependence of the conductivity σ, imaginary dielectric permittivity ε'', and real dielectric permittivity ε' for CCTO ceramics. According to our calculation, the measured conductivity in Fig. 1(a) is equal to the conductivity calculated from the dielectric function.

For the σ in Fig. 1(a), it should be noted that the experimental curves show two ranges of behavior. First, there is a strong rise at low frequencies. This is the grain-boundary blocking effect. Second, the conductivity does not increase as rapidly at high frequency. It is the bulk conductivity relaxation in which we are primarily interested. The σ in the second range can be described by "universal dielectric response" (UDR)[17,24]

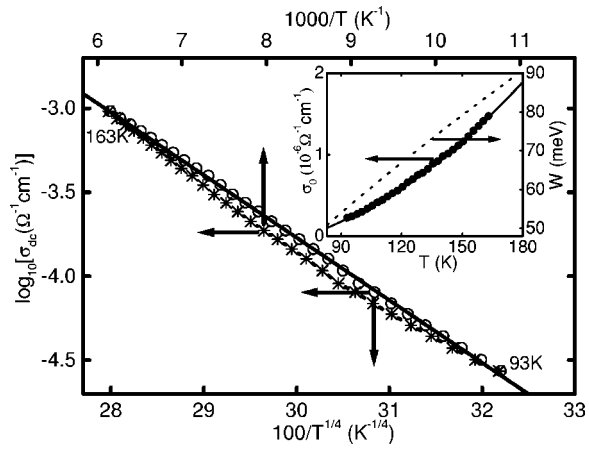

FIG. 2. Temperature-dependent dc conductivity σ_{dc} for CCTO ceramics scaled for thermally activated nearest-neighbor hopping of charges (stars, top and left axes) and VRH (open circles, bottom and left axes) (see the text). The solid line is the fitting curve of experimental data (open circles) according to Eq. (3). The inset displays the temperature dependence of the σ_0 (solid circles) and the W (the dashed line). The solid line in the inset is the result from Eq. (5).

$$\sigma = \sigma_{dc} + \sigma_0 f^s, \tag{1}$$

where σ_{dc} is the dc bulk conductivity, σ_0 is a constant, f is the frequency, and the exponent s is smaller than 1. Equation (1) is a common feature for all amorphous semiconductors and some other disordered systems.[17] It is typical of thermal assisted tunneling between localized states. In our system, it may be ascribed to the polaron relaxation.

This steplike increase in Fig. 1(a), which is accompanied by a loss peak in the imaginary part of the permittivity ε'' [Fig. 1(b)], shifts to higher frequencies with increasing temperature. The ε' decreases quickly in the same frequency range [Fig. 1(c)].

In Fig. 1(a), the dashed lines are the fitting curves of experimental results according to Eq. (1). The exponent s is about 0.33 in the entire measured temperature range. The temperature-dependent σ_{dc} is shown in Fig. 2.

Polaron relaxation means the existence of the UDR generally in a high-dielectric-constant material.[10] For a polaron relaxation, the σ is described by Eq. (1), and the frequency variation of the ε'' related to the relaxation follows a fractional power law in a wide frequency range at fixed temperature. It is $\varepsilon'' \propto f^{s-1}$. According to our fitting (not shown here), the high-frequency side of the experimental ε'' in Fig. 1(b) can be described by the expression well. The fitted value of the exponent s is 0.33, which is the same as the value obtained from the fitting process of σ. Therefore, the high-frequency behaviors ($f > f_r$) of σ and ε'' in CCTO are consistent with the polaron relaxation and UDR. Here, f_r is dielectric relaxation frequency.

In hopping conduction, the nearest-neighbor hopping obeys the Arrhenius-like law

$$\sigma_{dc} = \sigma_1' \exp(-E_a/k_B T), \tag{2}$$

where σ_1' is a constant, E_a is the activation energy, k_B the Boltzmann constant, and T the absolute temperature. Mott[23]

first pointed out that at low temperatures the most frequent hopping process would not be to a nearest neighbor. Then a Mott's variable-range-hopping (VRH) conductivity sets in. The VRH conduction mechanism can be described by the equation[23]

$$\sigma_{dc} = \sigma_1 \exp[-(T_0/T)^{1/4}], \quad (3)$$

where σ_1 and T_0 are constants and T_0 is given by

$$T_0 = 24/[\pi k_B N(E_F)\xi^3], \quad (4)$$

where $N(E_F)$ is the density of localized states at the Fermi level, and ξ is the decay length of the localized wave function. It is notable that the Arrhenius plot of the dc conductivity ($\log_{10}\sigma_{dc}$ vs $1000/T$) in Fig. 2 does not lead to a straight line over significant temperature ranges. In Fig. 2, the measured dc conductivity at low temperatures is plotted as a function of $\log_{10}\sigma_{dc}$ vs $100/T^{1/4}$. The solid line is the fitting curve of experimental data according to Eq. (3). The fitting parameters σ_1 and T_0 are 2.48×10^7 S cm^{-1} and 5.38×10^7 K, respectively. The two values of CCTO are similar to those of Li-doped La_2CuO_4 (Ref. 25) and Cu-doped $BaTiO_3$.[26] The VRH mechanism describes the bulk conductivity of CCTO ceramics well. It confirms that three-dimensional disorder effects dominate the conductivity of the semiconducting phase. VRH mechanism normally occurs in the low-temperature region (below room temperature) wherein the energy is insufficient to excite the charge carrier across the Coulomb gap. Thus Eq. (3) is a low-temperature expression. In the temperature range, conduction takes place by hopping of small region ($\sim k_BT$) in the vicinity of Fermi energy. Equation (3) fits the measured conductivity of CCTO well. It is a strong evidence for the existence of polarons in the CCTO.

The inset of Fig. 2 shows the temperature dependence of the σ_0 of Eq. (1). σ_0 increases quickly with increasing temperature. The solid line in the inset is the fitted curve of experimental data

$$\sigma_0 = -2.97\times10^{-7} + 2.23\times10^{-11}T^{2.21}(\Omega^{-1}\,\mathrm{cm}^{-1}). \quad (5)$$

Mott's VRH mechanism gives two relations[23]

$$W = 3/[4\pi R^3 N(E_F)], \quad (6)$$

$$R = \xi^{1/4}/[8\pi N(E_F)k_BT]^{1/4}, \quad (7)$$

where the W and R are the hopping energy and hopping range of polarons, respectively. According to Eqs. (4), (6), and (7), we obtain

$$W = 0.25k_B{T_0}^{1/4}T^{3/4}. \quad (8)$$

The inset of Fig. 2 shows the temperature dependence of the W values. The hopping energy W is 50 meV at 80 K. When the T increases to 180 K, the W increases to 90 meV monotonically. In Eq. (7), the hopping range R is related to ξ and $N(E_F)$. For $\xi\approx a=0.37$ nm, the distance between neighboring Ti ions of CCTO, this implies $N(E_F)\approx3.25\times10^{19}$ eV^{-1} cm^{-3} according to Eq. (4). The estimated R is 2.76 nm at 90 K. When the T increases to 180 K, the R decreases monotonically to 2.32 nm.

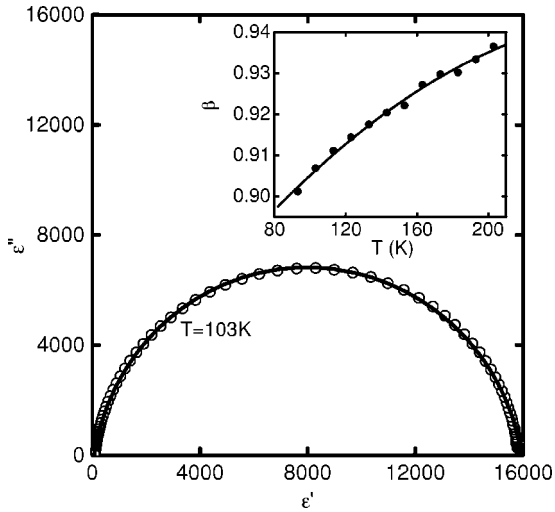

FIG. 3. Cole-Cole plot for CCTO ceramics at 103 K. Open circles are the experimental result; the solid line is the fitted result according to Eq. (10). The inset displays the temperature dependence of the β (solid circles). The solid line is drawn to guide the eye.

We studied the dielectric relaxation time distribution of CCTO simply according to the Cole-Cole equation[22]

$$\varepsilon = \varepsilon' - i\varepsilon'' \quad (9)$$

$$\varepsilon = \varepsilon_\infty + (\varepsilon_0 - \varepsilon_\infty)/[1 + (i\omega\tau)^\beta], \quad (10)$$

where ε_0 is the static permittivity, ε_∞ the permittivity at very high frequencies, ω the angular frequency, τ the mean relaxation time, and β a constant. Figure 3 shows the plot of the real part (ε') versus the imaginary part (ε'') of the complex permittivity, i.e., the Cole-Cole plot. The data fit well into a semicircular arc with the center lying underneath the abscissa. From the Cole-Cole plot and Eq. (10), we obtain the fitting results of ε_∞, ε_0, and β of CCTO. The ε_∞ and ε_0 are 70 and 15 900, respectively. They are independent of temperature in the measuring temperature range. The inset of Fig. 3 shows the temperature dependence of the β. With increasing temperature, the β increases slowly. Consequently, the relaxation time distribution has a monotonic decrease.

Figure 4 shows the temperature dependence of the relaxation frequency f_r in CCTO with a $\log_{10} f_r$ vs $100/T^{1/4}$ function, where f_r is obtained from the position of the loss peak in the ε'' versus $\log_{10} f$ plots. In the inset of Fig. 4, $\log_{10} f_r$ is plotted as a function of $1000/T$. The solid line is the best-fit curve of the equation

$$f_r = f_1'\exp[-E_r/(k_BT)], \quad (11)$$

where f_1' is the relaxation frequency at an infinite temperature and E_r the activation energy for the dielectric relaxation. The values for f_1' and E_r are 1.19×10^7 Hz and 67 meV, respectively. The value of the activation energy is in good agreement with that of pervoskite materials reported by Bidault *et al.*[21] It is notable that the relaxation frequency in the inset has a deviation form the Arrhenius behavior. Such a

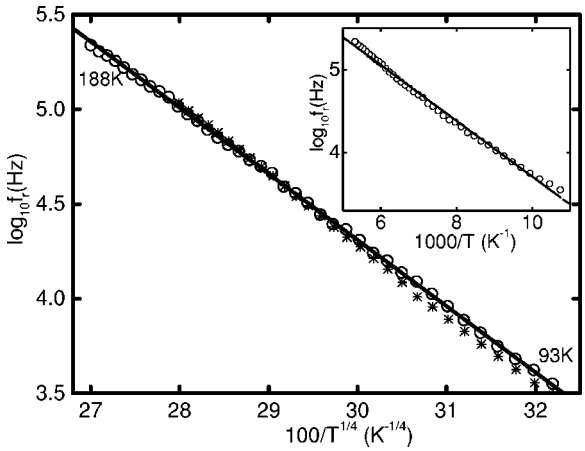

FIG. 4. Dependence of the relaxation frequency f_r on temperature ($\log_{10} f_r$ vs $100/T^{1/4}$). The open circles are the experimental results. The solid line is the best-fitting result according to Eq. (12). The stars are the calculated results according to Eq. (14). The inset displays the dependence of the relaxation frequency f_r on temperature ($\log_{10} f_r$ vs $1000/T$). The open circles are the experimental results. The solid line is the best-fitting result according to Eq. (11).

deviation can be found in the polaron relaxation of some materials [such as $Sr_{0.998}Ca_{0.002}TiO_3$ (Ref. 21)]. According to our calculation, the following relation can fit the f_r better

$$f_r = f_1 \exp[-(T_1/T)^{1/4}], \tag{12}$$

where f_1 and T_1 are two constants. The solid line in Fig. 4 is the fitting result of experimental results according to Eq. (12). The f_1 and T_1 are determined to be 5.02×10^{14} Hz and 4.04×10^{7} K, respectively. In the following part, we will show the f_r has a linear relation with the σ_{dc} approximately in our system. Thus it is not difficult to understand why the expression of Eq. (12) is different from the Arrhenius law, and is very similar to that of Eq. (3).

In Fig. 5, x-ray photoelectron peak shapes of the titanium $2p$ spectrum of the CCTO sample are shown. The Ti $2p_{3/2}$ peak is asymmetrical. It can be divided into the contributions from Ti^{3+} and Ti^{4+} by fitting the spectrum with two Gaussian-Lorentzian curves.[27] The curves we assigned as the Ti^{3+} and Ti^{4+} states have peak positions of 457.9 and

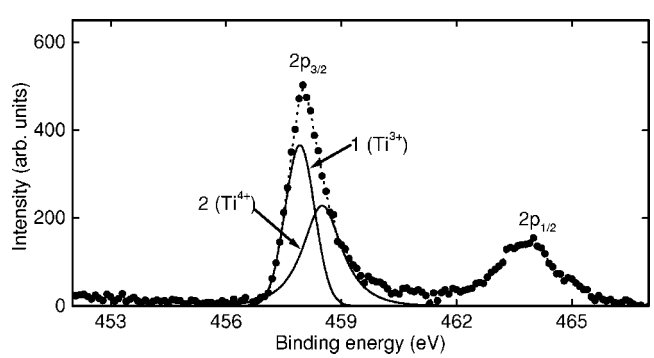

FIG. 5. XPS spectrum of the titanium $2p$ peak of CCTO ceramics. Curves 1 and 2 describe the contributions from the Ti^{3+} and Ti^{4+} states, respectively.

458.5 eV, which is within the range of published Ti^{3+} and Ti^{4+} $2p_{3/2}$ binding energies.[28] The x-ray photoelectron spectroscopic (XPS) analysis for the copper and calcium $2p$ spectrum shows that their states are Cu^{2+} and Ca^{2+}, respectively.

In CCTO, the Ti^{3+} and Ti^{4+} form Ti^{3+}-O-Ti^{4+} bonds. Under the applied field, the Ti-3d electrons in Ti^{3+} ions can hop to Ti^{4+}. The ionic radius (0.605 Å) of Ti^{4+} is smaller than that (0.670 Å) of Ti^{3+}. Thus the formation of Ti^{3+} ions will distort the lattice, and produce a polaronic distortion. The relaxation time of polarons is larger than that of free electrons attributable to the polaronic distortion. Meanwhile, under a dc applied field, the polaron can transport from a Ti^{3+}-O-Ti^{4+} to the other Ti^{3+}-O-Ti^{4+} as Ti^{3+}-O-Ti^{4+} bonds form a linked path. Consequently, a dc conduction will take place.

For CCTO, the origin of Ti^{3+} ions can be explained simply as the following. The existence of Ti^{3+} is compensated by the formation of oxygen vacancies. The oxygen vacancies occur due to the loss of oxygen from the grains during the high-temperature sintering. For CCTO ceramics, we have found an order-disorder phase transition of oxygen vacancies near 550 K according to the dielectric and transport measurements.[29] The activation energy of the dielectric relaxation related to the phase transition is about 0.41 eV. Recently, similar transition is also found in CCTO single crystal film.[30] The existence of the phase transition of oxygen vacancies shows that oxygen vacancies exist indeed in the lattice. Consequently, a mixed valence state of Ti ions will be induced.

In the above, the experimental results of the σ, ε' and ε'' of CCTO have been reported. We will use an equivalent circuit suggested by Lunkenheimer *et al.*[11] to explain the results. The inset of Fig. 1(c) shows the circuit. The C_1, G_1, C_2, and G_{dc} are boundary capacitance, boundary conductance, bulk capacitance, and bulk dc conductance, respectively. The conductance G_{UDR} is described by the frequency-dependent bulk ac conductivity $\sigma_{UDR}=\sigma_0 f^s$. The present circuit model does not include the contacts. It is due to two reasons: (1) The experimental impedance analysis of CCTO ceramics[16] shows that the contact effect does not exist. (2) A thin insulating aluminum oxide layer has been used[13] to separate the CCTO sample and electrode, and a giant dielectric constant ($\sim10^4$) is obtained. Thus it is speculated that the contact effect does not play a main role in the dielectric properties of CCTO.[5,13,16]

In the circuit of Fig. 1(c), we have $\sigma_b \ll \sigma_{dc}$, where σ_b is the boundary dc conductivity. This type of microstructure could be originated by the loss of oxygen from the bulk of the grains during the high-temperature sintering followed by a reoxidation of a surface layer at the grain boundary during the cooling-down process. Consequently, the density of polarons is high in the bulk, and is low at the grain boundary. The activation energy of polarons is lower than that of oxygen vacancies. At low temperatures, oxygen vacancies are frozen, and the polarons induced by oxygen vacancies respond to the conduction and IBLC effects.

In the fit using Eq. (1), we obtained σ_{dc}, σ_0, and s. According to the calculation about the circuit, we know that the zero-frequency and high-frequency dielectric permittivities of the system are C_1/C_0 and C_2/C_0, respectively. The C_0 is

TABLE I. Parameters used when fitting the low-temperature data in Fig. 1.

T (K)	σ_{dc} (S cm^{-1})	σ_0 (S cm^{-1})	σ_b (S cm^{-1})	s	ε_0	ε_∞
93	2.73×10^{-5}	2.23×10^{-7}	1×10^{-10}	0.33	15900	70
113	9.06×10^{-5}	4.84×10^{-7}				
133	2.74×10^{-4}	8.24×10^{-7}				
153	6.66×10^{-4}	1.22×10^{-6}				

the empty capacitance of the sample. In the fit using Eq. (10), we obtained ε_0 and ε_∞. Consequently, the C_1 and C_2 are obtained. Thus we need only fit a parameter σ_b in our calculation. As the fitting proceeded, we found that the circuit can describe the dielectric response of CCTO well for $\sigma_b < 1\times10^{-9}$ S cm^{-1}. When $\sigma_b < 1\times10^{-9}$ S cm^{-1}, the difference of the calculated results with different σ_b is negligible. It means the conductivity at the grain boundary is so small that the grain boundary is an insulating capacitor approximately. In Fig. 1, the solid lines are the calculated results of the equivalent circuit. In the calculation, we assume $\sigma_b = 1\times10^{-10}$ S cm^{-1}, which is in the range of $\sigma_b < 1\times10^{-9}$ S cm^{-1}. The calculated results are in good agreement with the experimental results. A complete list of the parameters used in the calculation is shown in Table I.

In Fig. 1(b), the increase of the temperature T moves the ε'' peak to the high frequency. Now we calculate the temperature dependence of the relaxation frequency f_r according to the circuit. At $f = f_r$, we have $\partial\varepsilon''/\partial f = 0$. Under this condition, one has the following relation:

$$\sigma_{dc} + \sigma_0 f_r^s = 2\pi f_r C_1. \tag{13}$$

In Eq. (13), the relaxation frequency f_r is related to σ_{dc}, σ_0, and s. In the fit using Eq. (1), we have obtained the σ_{dc}, σ_0, and s. Calculations showed that $\sigma_0 f_r^s$ was smaller than σ_{dc} at different temperatures for CCTO. Thus Eq. (13) can be written as

$$f_r \approx \sigma_{dc}/(2\pi C_1). \tag{14}$$

Here C_1 is a constant. Equation (14) means that f_r has an approximate linear relation with the σ_{dc}. In Fig. 4, the stars are the calculated f_r according to Eq. (14). It is in good agreement with the measured results. Based on Eqs. (3) and (14), Eq. (12) is obtained in approximation.

In the CCTO system, the ε' has a drop at low temperatures. It is intimately related to its semiconductor state. Figure 6 shows the temperature dependence of ε' at different frequencies. The curves show three ranges of behavior. First, there is a near-plateau range for $T < 80$ K, representing the "ground-state dielectric permittivity" ε_∞. In this temperature range, polarons are frozen. The bulk behavior in a grain is equivalent to an insulating capacitor. The total capacitance of a grain is C_2 approximately. Second, the dielectric permittivity in Fig. 6 has a strong rise near 100 K. It is related to the thermal excitation of the polarons. IBLC effects take place in this temperature region ($80\ \mathrm{K} < T < 200$ K). Finally there is another near-plateau range at higher temperature, representing the ε_0. The solid lines are the calculated results according to the circuit, Eqs. (3) and (5). The used parameters in circuit are the same values, which are shown in the above calculation. The calculated results are in good agreement with experimental results.

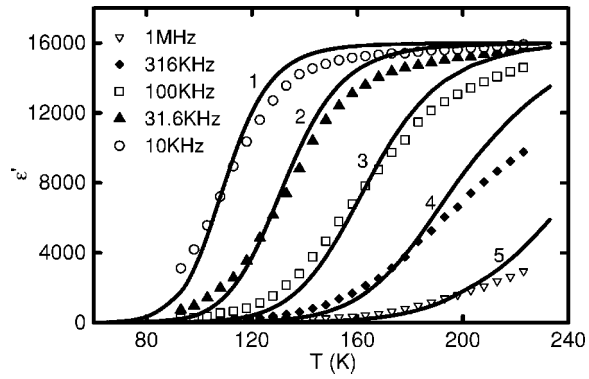

FIG. 6. Temperature dependence of the real dielectric permittivity ε' with different frequencies. The solid lines 1–5 are the calculated results according to the equivalent circuit. In the calculation, σ_1, T_0, σ_b, s, ε_0, and ε_∞ are 2.48×10^7 S cm^{-1}, 5.38×10^7 K, 1×10^{-10} S cm^{-1}, 0.33, 15 900, and 70, respectively.

IV. CONCLUSION

The ac bulk conductivity of CCTO shows a power-law behavior, which is consistent with a polaron relaxation. The dc bulk conductivity is found to obey Mott's VRH mechanism. The coexistence of Ti^{3+} and Ti^{4+} ions is the microscopic origin of polaron behaviors. The existence of Ti^{3+} is compensated by oxygen vacancies. The dielectric relaxation frequency in CCTO has a deviation from the Arrhenius behavior. It is related to the VRH mechanism. An equivalent circuit suggested by Lunkenheimer *et al.*[11] is used to explain the dielectric response of CCTO successfully. In this model, insulating layers inducing the giant dielectric phenomenon are assumed to be grain boundaries.

ACKNOWLEDGMENTS

We thank the Robert A. Welch Foundation for support. This work was also supported by the NSF-Career Program through Grant No. DMR-0092054 and an acknowledgment is made to the donors of The Petroleum Research Fund, administered by the American Chemical Society, for partial support of this research. L.Z. thanks his supervisor, Dr. P. Shiv Halasyamani, for his support to perform this work, and thanks Dr. Chong-Lin Chen and Dr. Quark Chen for helpful discussions.

[1] B. G. Kim, S. M. Cho, T. Y. Kim, and H. M. Jang, Phys. Rev. Lett. **86**, 3404 (2001).
[2] J. B. Wu, C. W. Nan, Y. H. Lin, and Y. Deng, Phys. Rev. Lett. **89**, 217601 (2002).
[3] M. A. Subramanian, L. Dong, N. Duan, B. A. Reisner, and A. W. Sleight, J. Solid State Chem. **151**, 323 (2000).
[4] A. P. Ramirez, M. A. Subramanian, M. Gardel, G. Blumberg, D. Li, T. Vogt, and S. M. Shapiro, Solid State Commun. **115**, 217 (2000).
[5] C. C. Homes, T. Vogt, S. M. Shapiro, S. Wakimoto, and A. P. Ramirez, Science **293**, 673 (2001).
[6] Y. Lin, Y. B. Chen, T. Garret, S. W. Liu, C. L. Chen, L. Chen, R. P. Bontchev, A. Jacobson, J. C. Jiang, E. I. Meletis, J. Horwitz, and H.-D. Wu, Appl. Phys. Lett. **81**, 631 (2002).
[7] W. Si, E. M. Cruz, P. D. Johnson, P. W. Barnes, P. Woodward, and A. P. Ramirez, Appl. Phys. Lett. **81**, 2056 (2002).
[8] C. C. Homes, T. Vogt, S. M. Shapiro, S. Wakimoto, M. A. Subramanian, and A. P. Ramirez, Phys. Rev. B **67**, 092106 (2003).
[9] L. He, J. B. Neaton, M. H. Cohen, D. Vanderbilt, and C. C. Homes, Phys. Rev. B **65**, 214112 (2002).
[10] L. He, J. B. Neaton, D. Vanderbilt, and M. H. Cohen, Phys. Rev. B **67**, 012103 (2003).
[11] P. Lunkenheimer, V. Bobnar, A. V. Pronin, A. I. Ritus, A. A. Volkov, and A. Loidl, Phys. Rev. B **66**, 052105 (2002).
[12] P. Lunkenheimer, M. Resch, A. Loidl, and Y. Hidaka, Phys. Rev. Lett. **69**, 498 (1992).
[13] A. P. Ramirez, G. Lawes, V. Butko, M. A. Subramanian, and C. M. Varma, cond-mat/0209498 (unpublished).
[14] M. H. Cohen, J. B. Neaton, L. He, and D. Vanderbilt, J. Appl. Phys. **94**, 3299 (2003).
[15] I. P. Raevski, S. A. Prosandeev, A. S. Bogatin, M. A. Malitskaya, and L. Jastrabik, J. Appl. Phys. **93**, 4130 (2003).
[16] D. C. Sinclair, T. B. Adams, F. D. Morrison, and A. R. West, Appl. Phys. Lett. **80**, 2153 (2002).
[17] S. R. Elliott, Adv. Phys. **36**, 135 (1987).
[18] Z. Yu, C. Ang, P. M. Vilarinho, P. Q. Mantas, and J. L. Baptista, J. Appl. Phys. **83**, 4874 (1998).
[19] O. Bidault, P. Goux, M. Kchikech, M. Belkaoumi, and M. Maglione, Phys. Rev. B **49**, 7868 (1994).
[20] L. Zhang, W. Kleemann, and W. L. Zhong, Phys. Rev. B **66**, 104105 (2002).
[21] O. Bidault, M. Maglione, M. Actis, M. Kchikech, and B. Salce, Phys. Rev. B **52**, 4191 (1995).
[22] C. Ang, Z. Yu, Z. Jing, P. Lunkenheimer, and A. Loidl, Phys. Rev. B **61**, 3922 (2000); C. Ang, J. R. Jurado, Z. Yu, M. T. Colomer, J. R. Frade, and J. L. Baptista, *ibid.* **57**, 11 858 (1998).
[23] N. F. Mott and E. A. Davis, *Electronic Processes in Non-crystalline Materials* (Clarendon, Oxford, 1979).
[24] A. K. Jonscher, *Dielectric Relaxation in Solids* (Chelsea Dielectrics Press, London, 1983).
[25] M. A. Kastner, B. J. Birgeneau, C. Y. Chen, Y. M. Chiang, D. R. Gabbe, H. P. Jenssen, T. Junk, C. J. Petters, P. J. Picone, T. Thino, T. R. Thurston, and H. L. Tuller, Phys. Rev. B **37**, 111 (1988).
[26] C. Ang, Z. Jing, and Z. Yu, J. Phys.: Condens. Matter **11**, 9703 (1999).
[27] *Practical Surface Analysis by Auger and X-Ray Photoelectron Spectroscopy*, edited by D. Briggs and M. P. Seah (John Wiley, New York, 1990).
[28] H. A. Bullen and S. J. Garrett, Nano Lett. **2**, 739 (2002).
[29] L. Zhang, K. M. Ok, and P. Shiv Halasyamani (unpublished).
[30] L. Chen, C. L. Chen, Y. Lin, Y. B. Chen, X. H. Chen, R. P. Bontchev, C. Y. Park, and A. J. Jacobson, Appl. Phys. Lett. **82**, 2317 (2003).